JOURNAL OF NANO- AND ELECTRONIC PHYSICS
Vol. **16** No 4, 04022(8pp) (2024)

ЖУРНАЛ НАНО- ТА ЕЛЕКТРОННОЇ ФІЗИКИ
Том **16** № 4, 04022(8cc) (2024)

OPEN ACCESS

REGULAR ARTICLE

Laser Surface Modification of the Wrought and LPBF-Printed Biomedical Co-28Cr-6Mo Alloys: Effects on nanoindentation and Tribological Behaviors

B.V. Efremenko[1,*], Yu.G. Chabak[1,2], V.G. Efremenko[1,2,3], F. Kromka[2], I.M. Olejnik[1], V.A. Shalomeev[4], E.V. Tsvetkova[1], A.V. Dzherenova[1]

[1] *Pryazovskyi State Technical University, 49044 Dnipro, Ukraine*
[2] *Institute of Materials Research, Slovak Academy of Sciences, 04001 Kosice, Slovakia*
[3] *International Research Institute for Steel Technology, Wuhan University of Science and Technology, 430081 Wuhan, China*
[4] *Zaporizhzhia Polytechnic National University, 69063 Zaporizhzhia, Ukraine*

(Received 28 May 2024; revised manuscript received 10 August 2024; published online 27 August 2024)

The object of this work is the effect of a laser beam surface treatment on the micro-mechanical and tribological properties of biomedical Co-28Cr-6Mo alloy manufactured by different methods (casting-forging or Laser Powder Bed Fusion (LPBF)). The wrought and LPBF alloys were superficially melted by the laser beam of 400 W power (fiber laser «TruFiber 400» (TRUMPF) of 1064 nm wavelength) under a scanning velocity of 5 mm·s^{-1}. The research was fulfilled using an optical (GX71 OLYMPUS) and electron scanning microscopy (JSM-7000F JEOL), X-ray diffraction (X'Pert PRO, PANalytical, Cu-Kα radiation), nanoindentation ("G200 Nano Indenter", Agilent Technologies) and tribological testing (a "Ball (Al_2O_3)-on-Plate" sliding in a simulated body fluid). It was found that laser treatment resulted in a modified (remelted) layer with a depth of 500-550 μm having mainly the α_{Co} phase (HCP) structure formed by dispersed dendrites. The dendrite cross-section size varied from 5-12 μm (in the primary arms) to 1.5-6.0 μm in the secondary arms; these values are much lower than the average grain size in the wrought unmodified alloy (44 μm). Laser treatment increased the hardness and yield strength of the wrought alloy by 23 % (to 5.21 GPa), and decreased the volume wear by 25 %. In contrast, laser surface melting hardly changed the micromechanical and tribological properties of the LPBF alloy since its structure was not refined relatively the as-printed (unmodified) state. However, the melting-induced densification (porosity elimination) of the modified layer was observed in the LPBF alloy thus indicating the positive effect of laser modification on the structure of the LPBD-manufactured components.

Keywords: Co-28Cr-6Mo alloy, Laser powder bed fusion, Laser beam melting, Sliding wear, Nanoindentation.

DOI: 10.21272/jnep.16(4).04022

PACS numbers: 42.62.Cf, 62.20.Qp, 61.66.Dk, 64.70.Kb

1. INTRODUCTION

Co-based alloys are well-known materials intended for applications under different extreme working conditions (high temperature, corrosion, severe wear, etc.) [1]. Among these alloys, Co-28Cr-6Mo alloy is the most famous and frequently applied in biomedical engineering due to its advanced combination of hardness, corrosion and wear resistance [2]. Co-28Cr-6Mo is manufactured as castings (ASTM F75) and wrought billets (ASTM F1537); in the last decade additive manufacturing has been increasingly used in its production [2, 3]. Co-28Cr-6Mo alloy is the first-option material for implants and structural elements in surgery, orthopedics, and dentistry [4]. Its special application is artificial joints (knee and hip) which work under sliding wear. The wear debris of Co-28Cr-6Mo may adversely affect the patient's health because of toxic ions Cr^{+3} and Co^{+2} which are released under sliding and accumulate in the tissue next to the joint [5]. This process results in "Adverse Local Tissue Reactions" manifesting in pain, swelling, and inflammation [6]. Therefore, increasing the durability of the Co-28Cr-6Mo alloy under friction conditions is an urgent task.

In this regard, different approaches to enhance the wear behaviour of Co-based alloys and other biomedical alloys are proposed including low-energy inert-gas ion bombardment [7], carbon ion implantation [8], coating deposition [9-11], etc. In [12, 13] the plasma-assisted technology of thermo-chemical treatment and surface hardening of the biomedical alloys were described. Amanov [14] used ultrasonic nanocrystal surface modification to harden Co-Cr-Mo alloy; the same approach was reported in [15] where the ultrasonic impact treatment was performed under cryogenic temperature leading to the formation of dislocation cell structures with a cell size of 200-700 nm.

In surface engineering, a laser treatment (LT) is reportedly highlighted as an effective way to control the

* Correspondence e-mail: efremenko_b_v@pstu.edu

Cite this article as: B.V. Efremenko et al., *J. Nano- Electron. Phys.* 16 No 4, 04022 (2024) https://doi.org/10.21272/jnep.16(4).04022

surface properties of different alloys [16]. High rates of heating and cooling, high energy density (allowing melting) make it possible to form structural states that are unattainable under conventional heat treatment conditions. In [17], LT with a surface melting was applied to the carburized LPBF Ti-based biomedical alloy that increased its hardness to 1000-1200 HV due to phase transformation and hard phases formation. However, currently, there is not enough data on the use of laser surface processing to improve the properties of Co-based alloys neither in wrought nor in LPBF conditions. Taking into account the above, the present work was aimed at studying the effect of laser treatment on micromechanical and tribological properties of biomedical Co-28Cr-6Mo alloy prepared by conventional (forging) and additive (LPBF) methods to reveal the effectiveness of LT depending on the manufacturing approach.

2. MATERIALS AND METHODS

The Co-28Cr-6Mo alloys fabricated by two technologies were the experimental materials. The wrought alloy was received from "Baoji Hanz Metal Material Co., Ltd.", in the form of a 100 mm diameter forged bar with a chemical composition: 29.70 wt% Cr, 5.85 wt% Mo, 0.15 wt% Ni, 0.10 wt% Si, 0.20 wt% C, 0.025 wt% Fe, Co – balance. The bar was cut by the precision cutting machine Baincut HSS ("Chennai Metco Pvt Ltd") to get the specimens of 5 × 10 × 25 mm size. As the alternative, Co-28Cr-6Mo was also fabricated by the Laser Powder Bed Fusion in the form of specimens of the above size. The LPBF process was fulfilled using a "ProX DMP 320" ("3D Systems") printer equipped with a 500 W fibre laser (1070 nm wavelength, 0.5 mm beam diameter). The powder feedstock was supplied by "Electro-Optical Systems" with an average particle size ≤ 63 μm. The chemical composition of the printed specimens (28.62 wt% Cr, 5.33 wt% Mo, 0.42 wt% Si, Co – balance) was detected by the optical emission spectrometer "Labspark 1000" (NCS).

The surface of the specimens was treated using the fiber laser TruFiber 400 ("TRUMPF") of 1064 nm wavelength. The process was performed in the open air under the following parameters: laser beam power of 400 W; laser beam spot diameter of 1.3 mm; scanning velocity of 5 mm·s^{-1}; track overlapping of 50 %; focus distance of 20 mm. The regime parameters were chosen based on numerical simulation to ensure surface melting. Laser-treated specimens were cooled at still air to the ambient temperature.

The microstructural study was performed on the mirror-polished specimens after the electro-etching in a 10 vol. % HCl solution under a 5 V voltage. The microstructure was observed employing the optical microscope (OM) GX71 ("Olympus") and scanning electron microscopy (SEM) EVO-MA15 ("Carl Zeiss") equipped with the energy-dispersive spectroscopy (EDX) detector INCAx-sight ("Oxford Instruments"). Phase constituents were identified by X-ray diffraction utilizing the diffractometer X'Pert PRO ("PANalytical") with Cu-Kα source. The Sage-Guillaud equation [18] was used to determine the volume fraction (VF) of the εCo (HCP) phase:

$$VF_{\varepsilon} = \frac{I_{(101)\varepsilon}}{I_{(101)\varepsilon} + 1.5 \cdot I_{(200)\gamma}} 100\%, \quad (1)$$

where $I_{(101)\varepsilon}$ and $I_{(200)\gamma}$ are the intensities of the corresponding peaks in the XRD pattern.

The micromechanical properties of the alloys were detected according to the nanoindentation procedure using "G200 Nano Indenter" (Agilent Technologies). Nanoindentation was performed by a Berkovich three-sided pyramid under the loading speed of 10 nm·s^{-1} to get the maximum penetration depth of 2000 nm. A hundred imprints were made with a 50 μm step in two rows to average the experimental results. From the nanoindentation test, the following parameters were derived: indentation modulus, indentation hardness, and plasticity index (PI). The latter was found as [19]:

$$PI = \frac{W_p}{W_t}, \quad (2)$$

where W_t is the total energy of nanoindentation ($W_t = W_e + W_p$); W_e and W_p are the elastic energy and plastic energy, respectively, defined according to ISO 14577-1 by the area under the "Load/Displacement" curve.

The yield strength ($YS_{0.2}$, MPa) was calculated by the equation proposed for Co-28Cr-6Mo alloy [20]:

$$YS_{0.2} = 3.2H - 526.6 \quad (3)$$

where H is a Vickers hardness.

The sliding wear behaviour was evaluated according to the "Ball-on-Plate" scheme utilizing the "Micron-tribo" tribometer (Micron-System) was utilized. The specimen (plate) was pressed by the Al_2O_3 ball of 3.0 mm diameter with a normal load of 5 N. The specimen made 5000 reciprocating movements (each 3.5 mm long) with a sliding speed of 7.0 mm·s^{-1} to pass the total sliding distance of 17.50 m. The test was performed at room temperature in a simulated body fluid (SBF) which is a water-based solution containing the ions with the following concentration (mM/liter): Na^+ of 145.0, Cl^- of 127.0, HCO^{3-} of 24.0, K^+ of 4.0, Ca^{2+} of 2.5, Mg^{2+} of 1.0. The sliding wear behaviour was evaluated using the volume loss (ΔV) and the mean coefficient of friction (CoF). The volume loss was measured as described elsewhere [3, 13]. The sliding tests were duplicated three times to determine the average ΔV value. The mean CoF value was calculated as the average of the CoF values derived from the individual strokes.

3. RESULTS

3.1 Microstructure Observation

Figure 1 depicts the microstructure of the as-received (unmodified) Co-28Cr-6Mo alloys. In the wrought alloy, the structure presents polyhedral-shaped grains of solid solution with an average size of 43.9±7.1 μm (Fig. 1a) [3]. The grain size is much smaller than the cast Co-28Cr-6Mo alloy indicating that grains were refined during the forging and subsequent heat treatment. At the same time, Fig. 1a

indicates the retaining of the dendritic structure: the grain boundaries are seen against the background of the dendrites formed under ingot solidification. As follows from the Backscatter Electron Image (BSEI) shown on the right side of Fig.1a, the dendrites have a darker contrast revealing a higher presence of chemical elements of lower atomic number. According to [3], the dendrites are enriched with $Co_{(Z=27)}$ (by 3.5 wt.%) while depleted with $Cr_{(Z=24)}$ (by 1.8 wt.%) and $Mo_{(Z=42)}$ (by 1.7 wt.%) (relative to the interdendritic areas). Carbide or intermetallic phases were not revealed in the wrought specimen's structure.

The microstructure of the LPBF-printed Co-28Cr-6Mo alloy consists of rows of tightly adjacent hemispherical elements with a radius of about 50-70 μm positioned perpendicular to the building direction (so-called "Fish-scale" pattern) (Fig. 1b). Each element is the melt pool appeared due to the melting of powder particles under the laser beam. The melt pool is composed of equiaxed cells and columnar grains positioned mainly along the heat flux direction inward of the specimen (Fig. 1c, left side). The cross-section of the cell (column) is about 0.3-1.0 μm (Fig. 1c, right side).

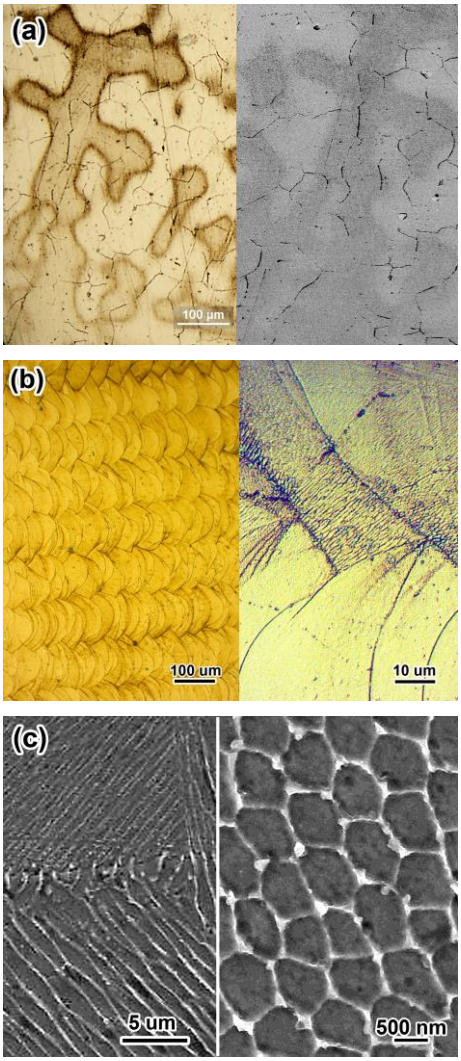

Fig. 1 – Microstructure of as-received Co-28Cr-6Mo alloys: (a) the wrought alloy (OM and SEM/BSEI), (b) LPBF alloy (OM), (c) LPBF (SEM/SEI). (SEI – secondary electron image)

After the laser scanning, the modified layer appeared on the surface having a similar mean thickness for the wrought and LPBF alloys (Figs. 2a and 2b). The layer consisted of overlapping hemispherical tracks (left after the laser beam movement) with a radius of 500-550 μm, referring to the maximum depth of the modified layer. The tracks presented the "melted-and-rapidly solidified" structure similar for both alloys. It consisted of butches of parallel dendrites oriented towards the surface, reaching tens and even hundreds of microns in length. In a cross-section, the dendrites were 5-12 μm in the primary arms, and 1.5-6 μm – in the secondary arms (Figs. 2c and 2d). Along the boundaries of the dendrites, precipitations

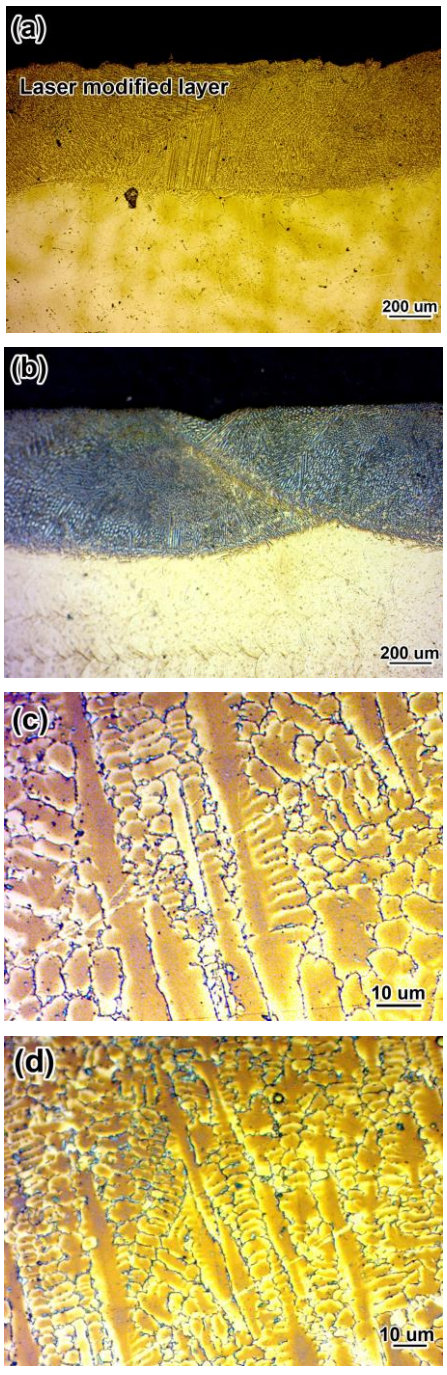

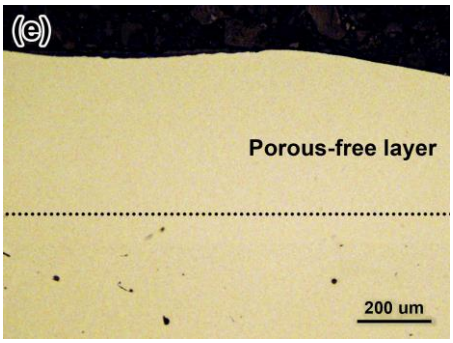

Fig. 2 – Microstructure of laser-processed Co-28Cr-6Mo alloys: (a, b) total view in cross-section, (c) non-etched structure, (d, e) the columnar grains within the laser-melted layer. (a, e – the wrought alloy; b, c, d – the LPBF alloy)

were observed in the form of a discontinuous thin network, which is presumably the σ-phase or carbide $(Cr, Co, Mo)_{23}C_6$ [21].

Figure 1e illustrates the non-etched structure of the LPBF alloy. It is seen that the laser-modified layer is porous-free although the bulk of the specimens has a porosity remaining after the LPBF alloy. The formation of a porous-free zone was due to laser-induced melting/solidification that allowed to elimination of the porous-like defects.

Figure 3 shows the XRD patterns of the as-received and laser-treated alloys. As seen, the peaks of γ_{Co}-based (FCC) and ε_{Co}-based (HCP) phases are present in all patterns. Following Equation (1), ε_{Co} is the main phase constituent in the wrought specimen (its volume fraction is 60.4 vol.%). In contrast, γ_{Co} is dominant in the structure of the LPBF alloy (with a volume fraction of 27.2 vol.%). After the laser treatment, the phase status of the LPBF alloy changed drastically in favor of the ε_{Co} phase: its volume fraction increased to 90.3 vol.%.

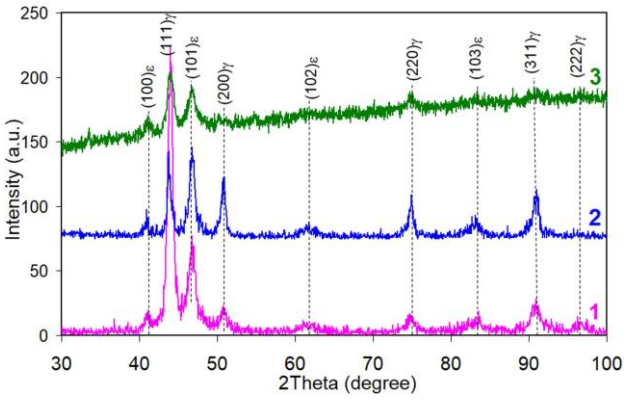

Fig. 3 – XRD patterns of Co-28Cr-6Mo alloys: 1 – as-received wrought, 2 – as-received LPBF, 3 – as-received LPBF + laser-melting

3.2 Nanoindentation Behaviour

Table 1 presents the results of the nanoindentation test of the Co-28Cr-6Mo alloys. Fig. 4 illustrates the representative "Load–Displacement" curves which refer to the mean hardness values of different alloys. In the case of the as-received wrought alloy, a much lower load (392 mN) was needed to attain the target indentation depth (2000 nm) compared with the as-received LPBF and the laser-treated alloys (Fig. 4a). This behaviour reflects a lower strength of the as-received wrought Co-28Cr alloy. In other cases, the curves practically overlapped each other, indicating the similarity in strength of the alloys.

As follows from Table 1, in the as-received state, the LPBF specimen had slightly higher indentation modulus as compared to the wrought specimen (243.47±3.9GPa and 237.53±5.2 GPa respectively) though the difference was statistically negligible. At the same time, the LPBF alloy demonstrated a significant advantage in hardness (5.17 GPa) and yield strength (1129 MPa) versus 4.24 GPa and 830 MPa of the wrought alloy, respectively. In contrast, the wrought alloy showed higher plasticity as follows from PI of 0.90 (versus 0.81 for the LPBF alloy).

The laser treatment hardly affected the strength indicators of the LPBF alloy however it noticeably (by 23%) improved the hardness and yield strength of the wrought alloy thus the latter was leveled with the LPBF alloy. Strengthening of the wrought alloy was accompanied by a decrease in its plasticity to PI of 0.82.

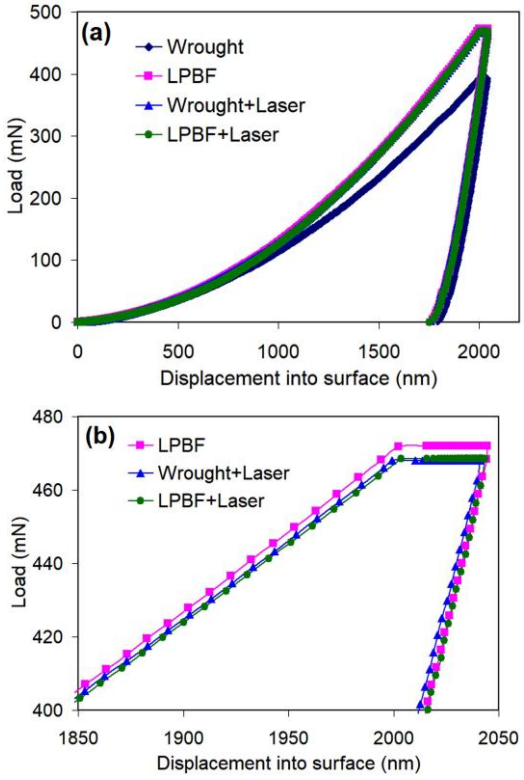

Fig. 4 – The characteristic "Load-Displacement" curves obtained during the nanoindentation test: (a) total curves, (b) the enlarged fragments of the curves

Table 1 – The mechanical properties of Co-28Cr-6Mo alloys derived from nanoindentation test (the experimental values scatter and the mean values)

Parameters	Wrought		LPBF	
	As-received	Laser-processed	As-received	Laser-processed
Indent. modulus (GPa)	224.01-252.11 (237.5±5.2)	207,07-228,11 (215,5±4.0)	217.07-242.22 (243.5±3.9)	223,02-245,39 (238,9±4.8)

Indent. hardness (GPa)	3.93-4.71 (4.24±0.1)	5.08-5.66 (5.21±0.2)	4.68-5.68 (5.17±0.2)	4.63-5.45 (5.09±0.1)
Yeild strength (MPa)	830	1141	1129	1102
Plasticity index (PI)*	0.90	0.82	0.81	0.82

*PI values were defined for the curves presented in Fig. 4.

After the laser melting, the indentation modulus decreased for both specimens, but to a greater extent for the wrought alloy. The possible reason is the residual stresses which decrease the elastic modulus [22]. The stresses may have a tensile character due to the contraction of a modified layer caused by: (a) its final cooling (thermal contraction) and (b) by γ_{Co} (FCC) $\rightarrow$ ε_{Co} (HCP) phase transformation. The latter leads to an increase in density (i.e. a decrease in a specific volume [23]) which ensures tensile residual stress occurrence.

3.3 Tribological Properties

The results of the wear tests are presented in Fig. 5-Fig. 7. After the testing, the wear tracks appeared on the surface shown in Fig. 5. The wear tracks were the grooves

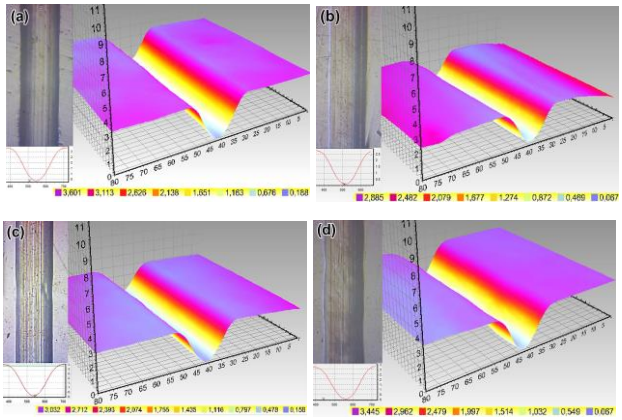

Fig. 5 – The wear tracks (in plane and 3D) on Co-28Cr-6Mo alloys' surface: (a) the wrought as-received, (b) the LPBF as-received, (c) the wrought laser-treated, (c) the LPBF laser-treated (the scale bar values are given in μm)

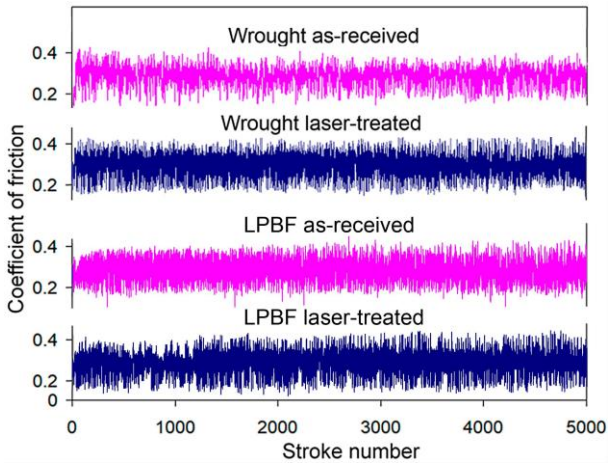

Fig. 6 – The CoF variations under wear testing

with smooth edges, without the beads of extruded metal on the sides, which indicated an increased surface strength. The tracks had approximately equal width (about 300 μm) and depth (~3 μm) except the track of the wrought (as-received) alloy. The latter had a greater depth (3.5-4 μm) which refers to a higher volume loss. As follows from Fig. 6, different alloys demonstrated similar variations of the coefficient of friction during the test: CoF values fluctuated within a range of about 0.15-0.4.

The mean values of volume loss and CoF are gathered in Fig. 7. In the as-received state, the LPBF alloy performed higher tribological properties as compared with the wrought alloy: it was manifested in lower values of volume loss (by 25 %) and the coefficient of friction (by 21 %). Laser processing led to a significant reduction in the volumetric wear of the wrought alloy: from 57.8×10^{-12} m^3 to 40.5×10^{-12} m^3, which approximately corresponds to the level of the as-received LPBF alloy. At the same time, the laser treatment hardly changed the wear resistance of the LPBF alloy as compared to the unmodified state. Thus, laser surface treatment caused an equalization of the wear resistance of the alloys. The same applies to the coefficient of friction: after laser treatment, both alloys showed approximately the same average CoF values of 0.23-0.24, which is close to that of the as-received LPBF alloy (0.26).

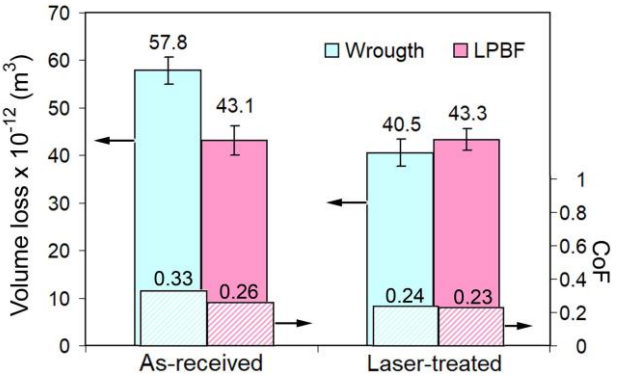

Fig. 7 – The mean values of volume loss and CoF of the wrought and LPBF Co-28Cr-6Mo alloys

4. DUSCUSSION

As studies have shown, the wrought and LPBF alloys in the as-received state, having a similar chemical composition, differed significantly in microstructure and properties (specifically, strength and wear resistance). This was caused by the manufacturing technology which strongly influenced both the phase composition and the sizes of the structural elements (dendrites, grains, cells). The structure of the wrought alloy was close to equilibrium since it mainly consisted of a low-temperature ε_{Co} phase (this resulted from the equilibrium structure formation at the stage of plastic deformation and heat treatment). Taking into account the revealed chemical segregation (dendrite-type structure, Fig. 1a), it can be assumed that the ε_{Co} phase mainly appeared in the interdendritic regions enriched in Mo and Cr, i.e. elements that stabilize the ε_{Co} phase of the epsilon phase [24]. In this case, the grains of the solid solution have a polygonal shape, characteristic of a diffusion

phase transformation under slow cooling rates.

In contrast, the LPBF alloy was formed at high crystallization rates (10^3-10^8 K/s [25]), which led to the formation of a dispersed cellular microstructure of a columnar type with a predominance of high-temperature (metastable) γ_{Co} phase. The reason for this may be the mechanical stabilization of the γ_{Co} phase by thermal stresses arising at high cooling rates. The mechanism of structure formation under LPBF is controlled by the G/R ratio, where G is the temperature gradient in the melt pool and R is the solidifying velocity [26]. Taking G and R values characteristic of the LBPF process, it was deduced [3] that the G/R value corresponds exactly to the "cellular mode" resulting in the columnar cells formation (observed in the LPBF Co-28Cr-6Mo alloy, Figs. 1b and 1c).

The ε_{Co} phase is known to be harder than the γ_{Co} phase due to the limited number of effective slip systems [27]. However, in our study, the LPBF alloy with a predominance of the γ_{Co} phase demonstrated higher strength properties (hardness, yield strength). This can be attributed to the Hall-Petch effect manifested due to the more dispersed structure of the LPBF alloy. Cell boundaries are actually the dislocation walls therefore they act as barriers for the gliding dislocations thus contributing ~ 330 MPa to the alloy's strength [3]. Furthermore, it was found that the cell boundaries in LPBF Co-28Cr-6Mo alloy are enriched in Mo and Cr [28] (the reason for segregation is a decrease in the elastic energy due to diffusional movement of Mo and Cr atoms to the dislocation cell boundary). This leads to an additional strengthening effect (up to 150 MPa [3]) caused by the local lattice mismatch around impurity atoms. Thus, the LPBF process creates a highly dispersed state of the alloy with an increased level of micro-stresses, which predetermines its higher nanohardness and yield strength as compared to the conventionally manufactured analogous. In contrast to the strength properties, the nanoindentation modulus of the LPBF and the wrought alloys differs slightly, within the statistical error. This is because the elastic modulus is determined rather by the interatomic bond strength in the Co lattice, than by the interaction of dislocations with obstacles during the deformation process.

As follows from the results obtained, the laser treatment equalized the structure and properties of the wrought and LPBF Co-28Cr-6Mo alloys. After the laser scanning, modified surface layers with a similar structure appeared in both alloys. The modified structure consisted of columnar dendrite-like crystals directionally solidified in a melt pool. The cross-section of the dendrites (1.5-6 μm in the secondary arms) is an order of magnitude smaller than the grain size in the unmodified wrought alloy. Accordingly, the laser melting significantly increased the hardness, strength, and wear resistance of the wrought alloy. It is noteworthy that wear resistance increased despite the fact that the sliding test was performed in a corrosive environment (SBF), which is known to activate wear due to tribocorrosion synergy [29]. In the LPBF alloy, on the contrary, the laser modification had virtually no effect on the hardness and wear resistance relative to the initial state. The reason is that laser melting of the surface did not result in a structure refinement. On the contrary: the cross-section size of the dendrites in the modified layer was 2.5-10 times higher than that of the cells in the as-printed LPBF alloy. This was caused by the differences in laser processing parameters applied to the LPBF process and laser surface modification.

The dimensions of the melt pool in the LPBF alloy (width 120-125 μm, depth of 40-50 μm – Fig.1b) correspond to the laser beam spot dimensions under 3D printing. During the laser surface modification, the beam diameter was 1.3 mm, and the depth of the melting pool reached 500-550 μm. If one considers the melt pool a sphere segment, then the volume of liquid metal in the melt pool can be approximately evaluated as 0.4 mm^3 (laser modification) and $3{\cdot}10^{-4}$ mm^3 (LPBF process). Taking the density of the Co-28Cr-6Mo alloy as 8.4 g/cm^3, this corresponds to the masses of the molten metal of about $3.4{\cdot}10^{-3}$ g and $2.5{\cdot}10^{-6}$ g, respectively. Such a big difference in the melt pool mass led to a crucial distinction in the solidification rate, affecting the sizes of structural elements (cells, dendrites).

In contrast to the LPBF process, the laser modification did not lead to preferentially γCo structure (as follows from the XRD study). This behaviour can be attributed to a lower temperature gradient (as compared with LPBF) and, accordingly, lower stresses, which were not sufficient for the mechanical stabilization of the γ_{Co} phase to martensitic FCC→HCP transformation.

The presented studies showed that laser processing in the surface melting mode differently affected the properties of the Co-28Cr-6Mo alloy depending on the alloy's manufacturing technology. The laser modification (through surface melting) is recommended to increase the strength and tribological characteristics of the Co-28Cr-6Mo alloy in the deformed or cast state. However, the laser modification is not so effective regarding the LPBF Co-28Cr-6Mo alloy. In the latter case, laser melting can be applied to densify the structure by eliminating the porous defects characteristic of LPBF-manufactured products.

CONCLUSIONS

The biomedical alloys Co-28Cr-6Mo, manufactured by various technologies (casting-forging and the LPBF process), were processed by a 400 W power laser beam with a scanning speed of 5 $mm{\cdot}sec^{-1}$. A modified layer was formed in the alloys to a depth of 700-750 μm. It consisted mainly of the ε_{Co} phase (HCP) with a structure of dispersed dendrites varying in the cross-section from 5-12 μm (in the primary arms) to 1.5-6 μm in the secondary arms. As a result, the hardness of the wrought alloy was increased by 23 %, and volumetric wear under the sliding in a simulated body fluid was decreased by 25 %. At the same time, laser modification did not have a noticeable effect on the properties of the LBPF alloy, because it did not lead to additional structure refinement as compared with an as-printed state. Laser treatment of the LPBF alloy in a melting mode is advisable only for increasing the density of the as-printed structure. In both alloys, the laser modification resulted in a decrease in a nanoindentation modulus, which may be ascribed to the occurrence of residual stresses in the modified layer.

ACKNOWLEDGMENTS

This research was supported by the Ministry of Education and Science of Ukraine (project No. 0123U101834). V.G. Efremenko and Yu.G. Chabak appreciate the support in the framework of the "EU Next Generation EU through the Recovery and Resilience Plan for Slovakia" under the project No. 09I03-03-V01-00061.

REFERENCES

1. T. Narushima, K. Alfirano Ueda, *Co-Cr Alloys as Effective Metallic Biomaterials*, In: M. Niinomi, et al. (Eds.), *Advances in Metallic Biomaterials*, Springer Series in Biomaterials Science and Engineering 3 (Springer-Verlag: Berlin – Heidelberg: 2015).
2. K. Dimitriadis, A.G. Lekatou, A.K. Sfikas, M. Roumpi, S. Tsouli, A. Galiatsatos, S. Agathopoulos, *J. Mater. Eng. Perform.* **30** No 7, 5252 (2021).
3. V.G. Efremenko, A.G. Lekatou, Yu.G. Chabak, B.V. Efremenko, I. Petryshynets, V.I. Zurnadzhy, S. Emmanouilidou, M. Vojtko, *Mater. Today Commun.* **35**, 105936 (2023).
4. Y. Chen, Y. Li, Y. Koizumi, H. Haider, A. Chiba. *Mater. Sci. Eng. C* **76**, 997 (2017).
5. Z. Xia, B.F. Ricciardi, Z. Liu, C. von Ruhland, M. Ward, A. Lord, *Nanomed. Nanotechnol. Biol. Med.* **13**, 1205 (2017).
6. F. Eltit, Q. Wang, R. Wang, *Front. Bioeng. Biotechnol.* **7**, 176 (2019).
7. M.O. Vasylyev, S.I. Sidorenko, S.M. Voloshko, T. Ishikawa, *Usp. Fiz. Met.* **3**, 209 (2016).
8. C. Liu, Z. Zhou, K.-Y. Li, *Electrochim. Acta* **241**, 331 (2017).
9. J. Corona-Gomez, K.K. Sandhi, Q. Yang, *J. Mech. Behav. Biomed. Mater.* **130**, 105228 (2022).
10. Z.A. Duriagina, I.A. Lemishka, A.M. Trostianchyn, V.V. Kulyk, S.G. Shvachko, T.L. Tepla, E.I. Pleshakov, T.M. Kovbasyuk, *Powder Metall. Met. Ceram.* **57** No 11-12, 697 (2019).
11. B.V. Efremenko, K. Shimizu, N. Espallargas, V.G. Efremenko, K. Kusumoto, Yu.G. Chabak, A.G. Belik, V.V. Chigarev, V.I. Zurnadzhy, *Wear* **460-461**, 203439 (2020).
12. Y. Dong, P. Svoboda, M. Vrbka, D. Kostal, F. Urban, J. Cizek, P. Roupcova, H. Dong, I. Krupka, M. Hartl, *J. Mech. Behav. Biomed. Mater.* **55**, 215 (2016).
13. Y. Chabak, B. Efremenko, I. Petryshynets, V. Efremenko, A.G. Lekatou, V. Zurnadzhy, I. Bogomol, V. Fedun, K. Kovaľ, T. Pastukhova, Materials **14** No 24, 7671 (2021).
14. A. Amanov, *Surf. Coat. Tech.* **421**, 127378 (2021).
15. M.O. Vasylyev, B.M. Mordyuk, S.I. Sydorenko, S.M. Voloshko, A.P. Burmak, N.V. Franchik, *Metallofiz. Nov. Tekhnol.* **39** No 7, 905 (2017).
16. L.V. Poperenko, V.V. Stukalenko, I.V. Yurgelevych, *J. Nano- Electron. Phys.* **11** No 3, 03032 (2019).
17. B.V. Efremenko, Yu.G. Chabak, E.V. Tsvetkova, A.V. Dzherenova, V.G. Efremenko, F. Kromka, V.I. Zurnadzhy, Olejnik I.M. *J. Nano- Electron. Phys.* **15** No 4, 04035 (2023).
18. M. Sage, C. Guillaud, *Rev. Met. Paris* **47**, 139 (1950).
19. A.M. Okoro, S.S. Lephuthing, L. Rasiwela, *Heliyon* **7**, e07978 (2021).
20. K. Ko, H.-G. Kang, Y.-H. Huh, C.-J. Park, L.-R. Cho, *J. Mech. Behav. Biomed. Mater.* **126**, 105051 (2022).
21. R. Rosenthal, B. Cardoso, I. Bott, R. Paranhos, E. Carvalho, *J. Mater. Sci.* **45**, 4021 (2010).
22. P. Galizia, L. Zoli, D. Sciti, *Mater. Des.* **160**, 803 (2018).
23. J.R. Davis, *Nickel, Cobalt and Their Alloys* (ASM International: Almere: 2000).
24. T.L. Achmad, W. Fu, H. Chen, C. Zhang, Z.-G. Yang, *Comput. Mater. Sci.* **121**, 86 (2016).
25. Y. Liu, A. Mace, H. Lee, M. Camargo, J.L. Gilbert, *Trib. Int.* **174**, 107770 (2022).
26. U.S. Bertoli, B.E. MacDonald, J.M. Schoenung, *Mater. Sci. Eng. A* **739**, 109 (2019).
27. A.J. Saldívar-García, H.F. L´opez, *J. Biomed. Mater. Res.* **74**, 269 (2005).
28. A. Mace, P. Khullar, C. Bouknight, J.L. Gilbert, *Dental Mater.* **38**, 1184 (2022).
29. O.V. Sukhova, V.A. Polonskyy, K.V. Ustinova, *Voprosy Khimii i Khimicheskoi Tekhnologii* **124** No 3, 46 (2019).

Лазерна модифікація поверхні кованого та виготовленого LPBF-друком біомедичного сплаву Co-28Cr-6Mo: вплив на наноіндентування та трибологічні властивості

Б.В. Єфременко[1], Ю.Г. Чабак[1,2], В.Г. Єфременко[1,2,3], Ф. Кромка[2], І.М. Олійник[1], В.А. Шаломеєв[4], О.В. Цветкова[1], А.В. Джеренова[1]

[1] *Приазовський державний технічний університет, 49044 Дніпро, Україна*
[2] *Інститут матеріалознавства, Словацька академія наук, 04001 Кошице, Словаччина*
[3] *Міжнародний науково-дослідний інститут технології сталі, Уханський університет науки та технології, 430081 Ухань, Китай*
[4] *Національний університет «Запорізька політехніка», 69063 Запоріжжя, Україна*

В даній роботі розглянуто вплив модифікації поверхні лазерним променем на мікромеханічні та трибологічні властивості біомедичного сплаву Co-28Cr-6Mo, виготовленого за різними технологіями: (а) лиття+гаряча деформація та (б) 3D-друк за схемою лазерного порошкового сплавлення (Laser Powder Bed Fusion – LPBF). Поверхню деформованого та LPBF зразків оплавляли лазерним променем потужністю 400 Вт при скануванні зі швидкістю 5 мм·с$^{-1}$ (використано волоконний лазер «TruFiber 400» (TRUMPF), довжина хвилі – 1064 нм). Дослідження проводили за допомогою оптичної (GX71, OLYMPUS) та електронної скануючої мікроскопії (JSM-7000F, JEOL), рентгенівської дифрактометрії (X'Pert PRO, PANalytical, Cu-Kα), наноіндентування ("G200 Nano Indenter", Agilent Technologies) та випробувань на зношування тертям за схемою "Ball (Al_2O_3)-on-Plate" в середовищі, що імітує рідину людського тіла. Встановлено, що лазерна обробка привела до

формування модифікованого (переплавленого) шару товщиною 500-550 мкм, що переважно складався із ε_{Co} (HCP) фази та мав дисперсну дендритну будову. Розмір дендритів у перерізі коливався від 5-12 мкм (у первинних осях) до 1,5-6,0 мкм – у вторинних осях, що набагато менше середнього розміру зерен у деформованому сплаві (44 мкм). Лазерна обробка підвищила твердість і межу текучості деформованого сплаву на 23 % (до 5,21 ГПа), а також зменшила його об'ємний знос на 25 %. В той же час, лазерна модифікація оплавленням практично не змінила мікромеханічні і трибологічні властивості LPBF сплаву, оскільки не відбулося подрібнення його мікроструктури відносно вихідного (немодифікованого) стану. Втім, лазерне оплавлення може бути корисним для 3D-друкованого Co-28Cr-6Mo сплаву, оскільки воно забезпечує ущільнення структури в модифікованому шарі шляхом ліквідації пористості, характерної для виробів, виготовлених за технологією LPBF.

Ключові слова: Сплав Co-28Cr-6Mo, Плавлення лазерного порошку, Оплавлення лазерним променем, Зношування тертям ковзанням, Наноіндентування.